Article

Flash Flood Susceptibility Assessment and Zonation by Integrating Analytic Hierarchy Process and Frequency Ratio Model with Diverse Spatial Data

Aqil Tariq [1] , Jianguo Yan [1,*,†] , Bushra Ghaffar [2] , Shujing Qin [3,*,†] , B. G. Mousa [4] , Alireza Sharifi [5] , Md. Enamul Huq [6] and Muhammad Aslam [7]

1 State Key Laboratory of Information Engineering in Surveying, Mapping and Remote Sensing, Wuhan University, Wuhan 430079, China
2 Department of Environmental Science, International Islamic University Islamabad, Islamabad 44000, Pakistan
3 State Key Laboratory of Water Resources and Hydropower Engineering Science, Wuhan University, Wuhan 430072, China
4 Department of Mining and Petroleum Engineering, Faculty of Engineering, Al-Azhar University, Cairo 11884, Egypt
5 Department of Surveying Engineering, Faculty of Civil Engineering, Shahid Rajaee Teacher Training University, Tehran 16788-15811, Iran
6 Key Laboratory of Integrated Regulation and Resource Development on Shallow Lake of Ministry of Education, College of Environment, Hohai University, Nanjing 210098, China
7 School of Computing Engineering and Physical Sciences, University of West of Scotland, Paisley G72 0LH, UK
* Correspondence: jgyan@whu.edu.cn (J.Y.); shujing.qin@whu.edu.cn (S.Q.)
† These authors contributed equally to this work.

Abstract: Flash floods are the most dangerous kinds of floods because they combine the destructive power of a flood with incredible speed. They occur when heavy rainfall exceeds the ability of the ground to absorb it. The main aim of this study is to generate flash flood maps using Analytical Hierarchy Process (AHP) and Frequency Ratio (FR) models in the river's floodplain between the Jhelum River and Chenab rivers. A total of eight flash flood-causative physical parameters are considered for this study. Six parameters are based on remote sensing images of the Advanced Land Observation Satellite (ALOS), Digital Elevation Model (DEM), and Sentinel-2 Satellite, which include slope, elevation, distance from the stream, drainage density, flow accumulation, and land use/land cover (LULC), respectively. The other two parameters are soil and geology, which consist of different rock and soil formations, respectively. In the case of AHP, each of the criteria is allotted an estimated weight according to its significant importance in the occurrence of flash floods. In the end, all the parameters were integrated using weighted overlay analysis in which the influence value of drainage density was given the highest weight. The analysis shows that a distance of 2500 m from the river has values of FR ranging from 0.54, 0.56, 1.21, 1.26, and 0.48, respectively. The output zones were categorized into very low, low, moderate, high, and very high risk, covering 7354, 5147, 3665, 2592, and 1343 km², respectively. Finally, the results show that the very high flood areas cover 1343 km², or 6.68% of the total area. The Mangla, Marala, and Trimmu valleys were identified as high-risk zones of the study area, which have been damaged drastically many times by flash floods. It provides policy guidelines for risk managers, emergency and disaster response services, urban and infrastructure planners, hydrologists, and climate scientists.

Keywords: remote sensing; GIS; AHP; FR; sentinel-2; DEM

1. Introduction

Due to climate change and other environmental factors, flood disasters have become the most frequent natural phenomenon. There is a significant threat to human lives worldwide because most countries are susceptible to flood hazards, which cause different

types of damage, like physical, social, and economic [1–5]. Although floods can inflict harm anywhere, the agricultural industry and infrastructure near rivers are the most vulnerable since floods affect agricultural land everywhere. This may be due to a lack of proper mapping or preventive measures or the involvement of different parameters like drainage density, slope, etc [6–10]. According to the past thirty years' disaster data, flooding is recorded almost every year in Pakistan [11,12]. The reasons behind the country's becoming a hazardous country are its extensive latitudinal extent, geographical location, the existence of three mountain systems in the country, a wide range of climate variations, and the earth morphology of the region [13–17]. Other than physiographic reasons, there are some other factors for susceptibility, which are the tremendous growth rate of the population, the massive population below the poverty line, the lack of disaster management actions (no accurate flood mapping) at the local and national level, the low economic growth rate of the country, and the absence of education for pre- and post-disaster management [18–21]. Disaster impacts are not uniformly distributed but have varying natures [22]. Susceptibility and disasters are directly proportional; higher exposure will result in the maximum effect of disasters. Following women, young people, and the disabled, the poorest people are the most affected because they don't have a lot of strength [23,24].

As part of recent climatic changes around the globe, the people of Chaj Doab have faced disasters and a diversity of natural calamities during the last couple of years, starting with an untimely snowfall in October 2004 all over the Chaj Doab. In the past ten years, sporadic disasters and emergencies have resulted from flash floods, land sliding, snow avalanches, and glacier lake outburst floods (GLOF), resulting in human life loss, animals, and partial deaths or complete damage to infrastructure [25–29]. Dominant parts of this infrastructure have been damaged beyond the restoration abilities of communities [30–34]. The susceptibility and hazard maps are significant in measures related to risk reduction in light of their general use in flood risk reduction. It also can organize, integrate, geo-visualize, and process spatial and non-spatial data from different sources [35–38]. Tributaries of the Jhelum and Chenab rivers drain primarily agricultural areas. During recent decades, the intensity and occurrence of floods have been expanded. This has raised the danger of damage to properties and loss of human lives [39]. In Chaj Doab, the recurrence of floods has extensively developed in the previous two decades because of worldwide environmental changes, climatic fluctuations, and human activities, specifically impromptu land cover and land use changes and infringement into the stream vicinity. As a result, the nation has confronted extreme flooding every year from 2010–2015, demonstrating that flooding has transformed into a yearly marvel [40,41].

Flood modeling studies with the collaboration of Geographic Information Systems (GIS) are used to spatially visualize floods of different return periods [42–50]. This integration also involves the Digital Elevation Model (DEM) used for elevation information [51]. Somehow, flood susceptibility assessment is applied to estimate the flood losses. Such kinds of studies are also used to evaluate the financial loss. Flood risk modeling is a central segment of flood risk reduction that aims to reduce the weaknesses of components in danger and has one key factor that decreases damage to some extent. Such an assessment is done through some other scientific measures [52]. It is essential in basin management and involves hydrologic models (precipitation, runoff, flood frequency, temperature, and rainfall interpolation), hydraulic models (drainage density, slope, land use, elevation, water percolation toward rocks and soil, flow accumulation, etc.), and mixing of all these physical parameters with the help of MCA-AHP. It generates very high to shallow susceptible zones [53]. GIS integration with hydraulic models is utilized for flood hazard evaluation and geo-visualization [54]. Satellite images (for example: SPOT/Sentinel and Landsat TM/MSS) are essential for proper flood zonation [55]. Remote sensing satellite data combined with GIS is effective and efficient in modeling flood risk, mapping floods, and identifying places and routes for evacuation. SRTM DEM or ASTER DEM/ALOSPALSAR are digital elevation models used worldwide for research-based projects, such as zonation and management and modeling of flood risk [56].

In the study area, the floodplain of the rivers Jhelum and Chenab is highly susceptible to recurrent flooding during the summer season. Almost every year, severe damage is caused to standing crops, infrastructure, and animal and human casualties. In the study area, population settlement is encroaching on potentially hazardous areas [57]. A considerable number of settlements are located next to the river catchment. Due to this, there is no adequate information for the municipal department, which causes a lot of environmental, economic, and social damage. Therefore, this study aims to carry out flood risk modeling and help reduce the losses resulting from recurrent flooding [58,59]. The primary purpose of this study is to analyze location-wise flood susceptibility and help reduce flood disasters in the Jhelum and Chenab Basins. This research also identifies the spatial pattern of flash flood hazards utilizing Analytic Hierarchy Process (AHP) and Frequency Ratio (FR) models. The findings of the FR, and AHP analyses were then used to discover and map flood risk zones in the study region, which was then used to develop a flood risk map for the region. The FR and AHP models were used to analyze the potential flood-prone locations in the study area. These findings will be helpful to planners, researchers, and the local government for impact assessment, which will allow them to anticipate flood zones in the future and decrease the danger of flooding by devising various mitigation techniques. Because of this, the researchers employed FR and MCA in conjunction with AHP to develop flash flood hazard zonation, which was used to describe high-risk locations and determine the most significant component responsible for flash floods in the research area. It also makes recommendations to policymakers or local governments on flood risk management policies. The goal of this study was to check the accuracy of flood maps and see if they can help with disaster management by looking at the ground beneath them. Thus, it will give policymakers advice on dealing with flood hazards, especially in Chaj Doab [60].

2. Study Area

Chaj Doab encompasses the region bounded by the Jhelum and Chenab Rivers, respectively. It may be found between 73°30′ and 74°28′ E and 32°7′ and 33°30′ N (Figure 1). Located on the valley's southern outskirts, it is part of Kashmir. Districts Gujrat, Mandi Bahuddin, and Sargodha make up this region. River flooding is a significant problem in Pakistan because of the monsoon rains and melting snow that cause Pakistan's rivers to overflow their banks. The total study area is 20,101 km^2. Three significant rivers generate flooding in Pakistan: the River Jhelum and the River Chenab [61]. Pakistan's economy relies heavily on water from the upper Jhelum River, which drains the southern slopes of the Himalayas and Pir Panjal. Pakistan's Chenab River is a significant tributary of the Indus, one of the Indus basin's greatest rivers [62].
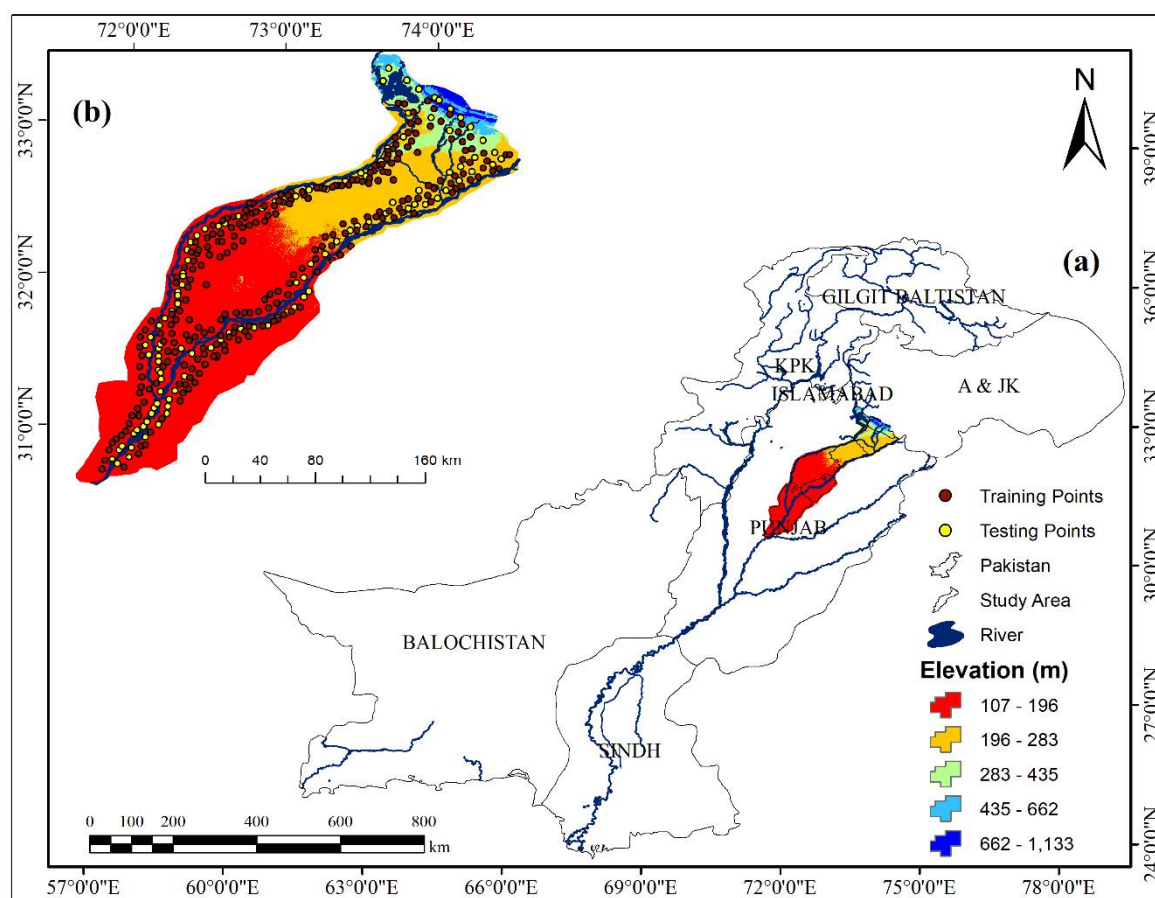
Figure 1. In this study, (**a**) indicate where study area is exists in Pakistan (**b**) Location of study area and the experts employed a variety of training and testing locations, which may be seen on a map.

3. Collection and Preparation of Data

3.1. Inventory of Flash Flood Zoning

While the study area is more significant than one L band, the site is not covered with one DEM layer. It is covered with 10 L-band PALSAR layers that are downloaded. In this analysis, 300 flood and non-flood points were randomly chosen from the flooded region and low-flood-likelihood high-altitude areas used for training and testing data sets (Figure 1). These points were split into 70% for training data points and 30% for testing data points [56].

3.2. Flash Flood Conditioning Factors

A total of nine flash flood influencing characteristics, including river distance, aspect, and elevation of the riverbank, slope, rainfall, and distance from the streams, soil types, LULC, and geology, were modeled in this research. ArcGIS 10.8, ENVI 5.4, and SAGA-GIS 2 were used to create thematic maps (Figure 2). Geology and soil data were collected from Punjab, Pakistan's geological and soil survey. These events depend on many factors, including the distance from the river, drainage density, slope, elevation, rainfall, soil, geology, and land-use/cover activities. Plan the inventory of flash floods and forecast possible flash flood events. These flash flood conditioning factors are essential.

Figure 2. Flash flooding with damage caused in the study area.

Various ArcGIS tools were used to create flood risk maps and assessments. This is why ArcGIS tools and methods were used to predict flood risk by utilizing spatial data from the ArcGIS database. This study's analysis emphasized the primary and secondary data sources. Using the Google Earth Engine, we could get a lot of the initial data. Obtaining the relevant data was a crucial step in solving this challenge. In this study, we aquired meterlogical and hydrological data from the Pakistan Meterological Department (PMD), Punjab, Pakistan (https://www.pmd.gov.pk/en/ (accessed on 26 August 2021). Besides, meterological data we obtained the primary geological and soil data from the soil survey department Pakistan (https://gsp.gov.pk/) (accessed on 2 October 2021). The Alaska Satellite Facility (ASF) provides a PALSAR Phased Array type L-band DEM (Digital Elevation Model) with a resolution of 12.5 m (https://vertex.daac.asf.alaska.edu/) (accessed on 18 November 2021).

Natural disasters, such as floods, landslides, and cyclones, mainly depend on several conditions. Choosing is often a complicated challenge to select parameters to create flood susceptibility maps [58]. Therefore, a field survey was conducted to determine the most relevant flood-triggering variables. The most flood-prone areas were visited during a month-long field visit in 2015. Residents' personal opinions were collected, which played a constructive role in planning the inventory map. A total of eight parameters, namely, distance from the river, drainage density, slope, elevation, rainfall, soil, geology, and land use land cover (LULC), were included in the modeling in this report.

To meet the requirements of model studies, these maps were transformed into raster images (formats) of 12.5 m by 12.5 m pixel size (Table 1). Below is a more in-depth explanation of each of these elements. The cell size of each parameter was kept at 12.5 m in the resampling method such that the overlay analysis would get the pixel at the same scale, and the output would also be the same as the input. The maps acquired at different scales were digitized, and while converting them to the raster format, the resolution of the pixels was kept at 12.5 m. keeping the resolution at 12.5 m for all raster parameters matched the pixel size. Most of the parameters were extracted from the DEM with a resolution of 12.5 m, and all other parameters were brought to the same resolution. Below is a comprehensive overview of the mentioned variables.

Table 1. The sources from where different data were collected and their purpose of application.

S. No	Primary Data	Spatial Resolution	Format	Source of Data	Derived Map
1	Sentinel-2	10 m	Raster	(https://earthexplorer.usgs.gov) (accessed on 11 June 2021).	Land Use Map, extraction of drainage basin
2	ALOS-PALSAR (DEM)	12.5	Raster	https://search.asf.alaska.edu/ (accessed on 18 November 2021)	Slope, Drainage density, Elevation, Flow accumulation Distance from river
4	Geological Data	1:10,000	Vector	https://gsp.gov.pk/ (accessed on 2 October 2021).	Geological Map
5	Soil Data	1:100,000	Vector	https://soil.punjab.gov.pk/ (accessed on 10 August 2021).	Soil Map
6	Rainfall Data	1:100,000	Raster	https://www.pmd.gov.pk/en/ (accessed on 26 August 2021)	Rainfall Deviation map

3.2.1. Slope

Many factors affect catchment hydrologic characteristics, which ultimately influence surface runoff production. It governs overland movement, penetration, and subsurface flow length [63,64]. When it comes to terrain stability, the slope is critical. The slope's gradient influences the volume and direction of surface runoff and subsurface drainage that reach a location. The slope heavily influences precipitation's contribution to streamflow: it controls overland, subsurface, and infiltration flow duration. The link between the slope's shape and the lithology, structure, type of soil, and drainage system is primarily defined by slope angles. It is preferable to have a rougher surface that slows down the flood response rather than a smooth or flat surface that enables water to flow more rapidly. Surface runoff is more likely to occur on steeper slopes, while water logging is more likely on flat terrain (Figure 3a). Slopes with a low gradient are more susceptible to flooding than slopes with a high gradient. In a region where the slope gradient usually is low, rain or extra water from the river constantly congregates. Water cannot accumulate and cause flooding in areas with steep slopes. River-induced floods are more likely to be caused by differences in DEM cell elevations, while pluvial floods are more likely to be produced by local depressions [65]. This suggests that the way elevation is linked to risk is critical.

3.2.2. Elevation

Lower elevation DEM cells would be of more importance. Elevation information shows how the stature of the ground changes over a region. This information is critical in creating flood maps, as these elements are widely accepted to impact flood mapping directly [66]. They give us the chance to model, investigate, and show wonder. The ALOSPALSAR DEM has been used to extract various interims. The raster map in Figure 3b shows the elevation map for Jhelum and Chenab.
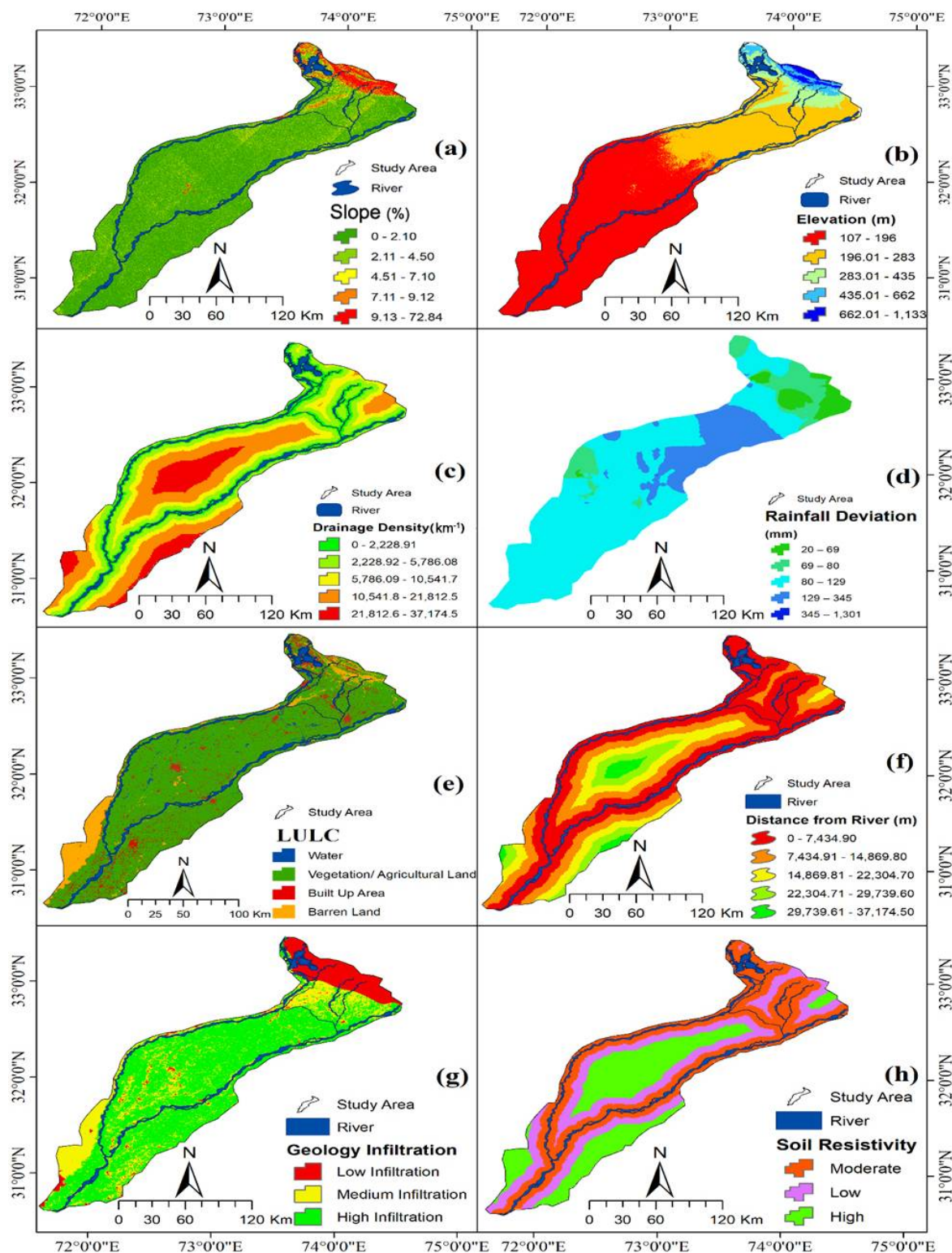
Figure 3. In this study, maps of flash flood conditioning variables were used: (**a**) slope, (**b**) elevation, (**c**) drainage density, (**d**) rainfall deviation, (**e**) LULC, (**f**) distance from the stream, (**g**) geology infiltration, and (**h**) soil resistivity.

3.2.3. Drainage Density

The total length of the stream network per unit area is how drainage density is described. Following Strahler's [58] approach to stream ordering, heavier weights were allocated to places with low drainage density, and lower weights were assigned to those

with enough water supply. It was determined that three major rivers in the research region were more dangerous due to the area's buildup of flow. The drainage density layer was subdivided into five distinct categories. Following the normal categorization Schemes 1–5 in the Figure 3c. Figure 3c shows how the findings classified areas with extremely low drainage densities as five and areas with very high drainage densities ranked as 1. Using AHP, we calculated density as the second most significant metric using kernel density that found the river density within a 500-m radius. This was done by utilizing equal interval ranges of five risk groups for those raster pixels. They discovered that river densities are highest around the Jhelum and Chenab Rivers and where those rivers meet the Trimmu Barrage. Water absorption capacity diminishes as density rises, so a flash flood is more likely to occur when the water is more vulnerable to land cover (Figure 3c).

3.2.4. Rainfall Deviation

Flood susceptibility and heavy rainfall are both positively correlated with flood occurrences. The rainfall rate rises from July to September for the study region, and in this way, flooding months are detected, i.e., sessions of monsoon in the Chaj Doab. In estimating flood types that are flashy, rapid, and of short duration, the amount of surface runoff is critical due to heavy rainfall [67]. Here, the variance in rainfall was regarded as an initiating factor for the study of flood susceptibility because a positive deviation in rainfall can cause floods. In contrast, a negative deviation in rainfall causes a shortage of rainfall, leading to the possibility of drought. The rainfall deviation was calculated based on the data of five rain gauge stations, i.e., Wazirabad, Jhelum, Mandi Bahuddin, and Gujrat. The inverse distance weight (IDW) interpolation technique was used in ArcGIS to map rainfall deviations for Chaj Doab (Figure 3d). To estimate variance and spatial mapping, the annual average with reported annual precipitation of the Chaj Doab was taken from 2010 to 2015. Equation (1) was used to determine how much rainfall was different from the average for each rain gauge station.

$$Q = \left(\frac{(L - Z) \times 100}{z} \right) \tag{1}$$

where L is the recorded rainfall, Z indicates the average rainfall, and Q represents the rainfall deviation.

3.2.5. Land Use and Land Cover

Flood hazard mapping also considers land-use and land-cover management since this is one component that represents the current usage of the land, its pattern and type, and its value in connection to soil stability and infiltration. Soil water storage capacity is strongly influenced by land covers, such as permanent grassland or other crops growing on it (Figure 3e). In contrast to areas with a thick layer of vegetation, rainfall runoff is far more common on bare ground. The presence of lush vegetation delays the water's trip from the sky to the soil and lowers runoff. On the other hand, concrete has a shallow water absorption rate since it is an impervious surface. Soil penetration capacity is reduced, and water runoff increases due to land use such as buildings, roads, and slum areas. Therefore, land-use types act as protective coverings that reduce the time it takes for water to accumulate; this, in turn, raises the peak discharge of water and contributes to a more severe flood. It follows that land use and land cover are essential determinants of flood probability (Figure 3e).

3.2.6. Distance from the Stream

In normal and flash flood situations, the land along the rivers is more vulnerable to flooding because the water flows from higher altitudes and accumulates at lower elevations in the river basin. Dams, ponds, lakes, and the land surrounding them frequently become inundated during periods of particularly severe rain. On top of all that, the land around

waterways tends to be flat. More than 2500 m was deemed the most vulnerable area, whereas more than 10,000 m was regarded as safe (Figure 3f).

3.2.7. Geology

Basin geology affects hydrological response. Soil permeability is the most important geological property for surface runoff. The ability of impermeable soil to permeate causes rapid and deep surface runoff. Looking at Figure 3g, you can see that the geology in the lower parts of the study area includes Jhelum Slate, conglomerate, and Koghuzi Greenschist. These types of rocks have low infiltration and more chances of flooding. The geology and soil of the area of interest were collected from Pakistan's Geological and Soil Department Survey. Each layer of spatial data in the occurrence of flood events is examined using rock formation and soil permeability. Each class parameter has been assigned a weight, and then selected parameters are added to create a flood susceptibility guide.

3.2.8. Soil

A soil's most critical elements and qualities are its texture and moisture content. Soil textures significantly affect floods because sandy soil absorbs water quickly and produces little runoff. In contrast, clay soils are less permeable than sandy soils and retain more water. Thus, flooding is more likely to occur in locations with clayey soils. Soil properties such as structure and infiltration capacity have a significant role in how well soils absorb water. Soil types vary widely in their ability to hold water. Decreases in soil infiltration capacity lead to an increase in surface runoff, which raises the risk of flooding. Runoff from the sloping ground may lead to floods if the water supply exceeds the soil's infiltration capacity. Figure 3h shows how the soil map was categorized based on how much water could be absorbed by the soil for this case study. There are three basic kinds of soil in the municipality: highly contaminated, moderately contaminated, and less contaminated soil. To create a weighted soil map, each soil class was assigned a certain weight, with the soil type with the most potential for flooding rated 3 and the one with the least being ranked 1. In the form of a graphic picture, the soil factor findings in the research area are given.

4. Methods and Methodology

This study focuses on research techniques and research frameworks. It provides information on the instruments and procedures used to get the data. Flood risk mapping and assessment were developed using a variety of capabilities in the ESRI ArcGIS software. Following flood risk mapping, ArcGIS tools and methodologies were used to perform spatial data flood modeling. This model's geographic data helped flood managers develop good suggestions for reducing flood risk in the future [68].

The following are some of the most important phases in the study methodology: Specifically, (1) data collection and preparation, (2) dataset development for training and testing, (3) AHP modeling and the selection of class weight values, (4) SCWV and FR models, (5) validation of the models, and (6) generation of flash flood susceptibility maps are all included (Figure 4). These procedures are discussed in further depth in the sections that follow.
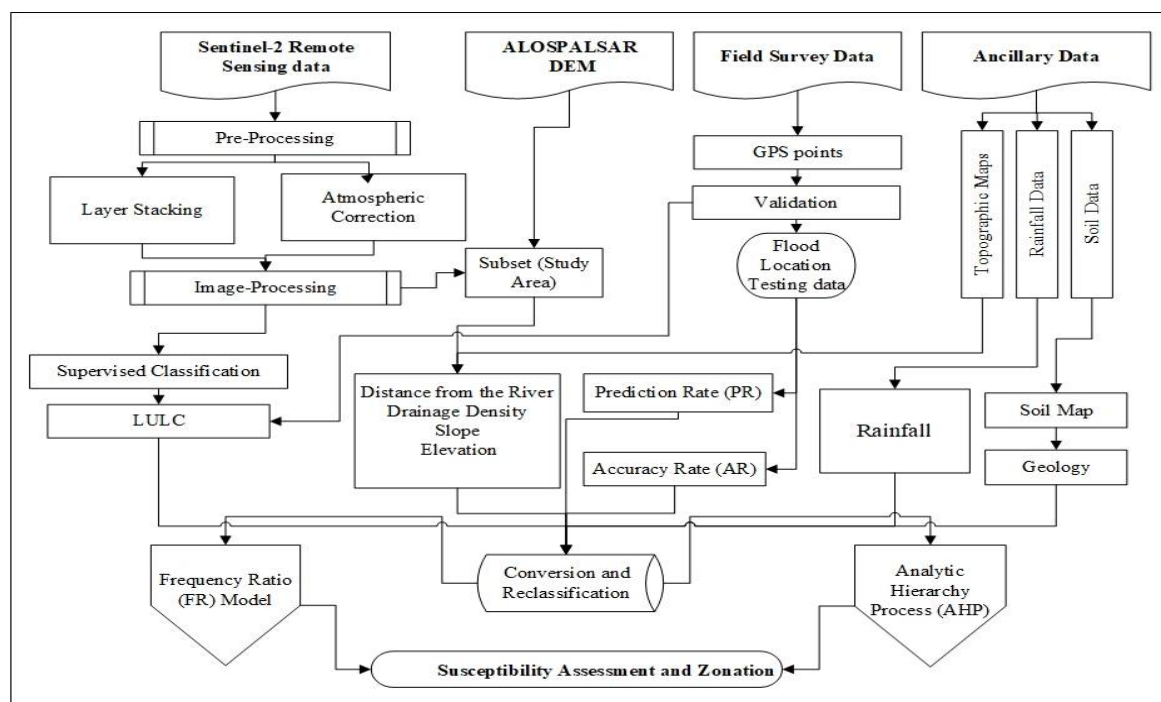
Figure 4. Flow chart of the methodology used in this study.

4.1. Collection of Data and Its Preparation

Inventory maps of flash floods and the conditioning factors were produced in the raster format with a 12.5 m pixel size. The frequency ratio values of every conditioning factor class were then calculated using the frequency ratio method. The inventory map was then overlaid with the conditioning factor maps. The weights of the class of variables were then calculated using the frequency ratio values. In flash flood modeling, selecting correlation-based features were used to determine the essential factors and determine how important these factors were.

4.2. Training and Testing Datasets' Generation

The susceptibility to flash floods was divided into two sections with 70% and 30% ratios. Among these elements, 70% of the susceptibility data was used to sample the conditioning factors assigned to the training dataset generation weights. The remaining 30% was used to sample the conditioning factors set to the weights for the evaluation dataset generation. The collection ratios can influence a model's efficiency regarding the training division and test inventory. The ratio of 70/30 was used in this analysis as it is a typical ratio used in modeling [69,70]. These steps were carried out in the ArcGIS 10.8 environment.

4.3. AHP Modeling and the SFWV

The present research has focused on developing susceptibility maps requiring physical parameters. Different analytical and decision-making processes are used to develop such maps. For the evaluation and development of the flood zonation maps, the Analytical Hierarchal Process (AHP) was used. While using this process, first, the values for each factor were calculated. These calculations were made through summation and division, and finally, the resultant values were assigned weightage [59]. Certain specific parameters were used in the application of this AHP modeling. In this instance, the AHP method was used to develop the zonation maps. The techniques used by applying the AHP-method were more efficient and rational. These AHP method techniques were combined with ArcGIS techniques to develop the required maps.

In the present analysis, the AHP approach was used to help the judgment by comparing the selected flood-causing variables by calculating the selected factor weight values (SFWVs). A survey of residents was conducted, and observations from the field were made to understand the relative significance of various flood factors in the study area and position them in their rank based on given preferences. The challenge in AHP can be described as determining how to assign weights, ranks, or significance to a collection of alternatives based on their likelihood of occurrence in specific situations. One of these variables was calculated based on a numerical scale (Table 2) [71].

Table 2. Comparison of two factors that can induce flooding in the form of a numerical scale.

S. No	Explanation/Definitions	Importance Intensity
01	Extremely more important	8 and 9
02	Very strongly more important	6 and 7
03	Strongly more important	4 and 5
04	Moderately more important	3 and 2
05	Equally important	1

An analysis of the flood variables' meanings or relevance was conducted, and a pairwise comparison matrix was constructed. Values were assigned to each rank on a scale from 1 to 9 based on the seven total flood-causing factors selected. Each of these weights was allocated depending on how significant they were in this particular event. The value given to one choice was equal to the common value assigned to the other choice (1/2 to 1/9).

The eigenvector of weight factor values was examined and changed by calculating the consistency ratio for the hierarchical arrangement of flood-causing components using the AHP method (CR) [72,73]. To examine the accuracy while taking importance into account, factor weight values for categorized sub-factors were generated once each factor's relative rank was determined. Equation (2) was used to calculate the eigenvector:

$$Ax = \lambda max^X \tag{2}$$

where λ is the eigenvalue of the criterion, x is the eigenvector of the criteria, and A is the comparison matrix of the n criteria. In the case of a stable reciprocal matrix, the maximum eigenvalue (max) equals the number of comparisons (n). For this reason, it is essential to figure out the consistency ratio (CR) for each case in question. Saaty [74] proposed that if the CR exceeds "0.1", the judgment collection is "inconsistent" and has to be reproduced and that this is the case. For example, if the CR is equal to "0", the choice is consistent; furthermore, any number between 0 and 0.1 is commonly referred to as consistent [74]. To calculate the ratio of consistency, use the following Equation (3):

$$CR = \left(\frac{CI}{RI}\right) \tag{3}$$

Using CR as the basis, we can get a consistency index of CI and a random index of RI from that value. RI was taken from [45]. However, CI was calculated using Equation (4):

$$CI = \left(\frac{\lambda max - N}{N - I}\right) \tag{4}$$

where the overall number of sub-factors is λmax, which is equal to the average of x criterion, and N is the total number of sub-factors AHP has the potential to be applied in a variety of fields where multiple factors are responsible for the occurrence of an incidence, such as ecotourism assessments [46], the selection and evaluation of industrial land use [46], the evaluation of residential LULC suitability [45], post-harvest technology selection [68],

irrigation network maintenance [72], selecting the most appropriate underground mining technique [75], and disease risk mapping and transmission [58].

4.4. FR Model and the SCWV

Frequency Ration (FR) is one of the most often used bivariate analytic approaches in flood risk assessments. FR is a form of bivariate statistical research based on the spatial connection between dependent and independent variables. This research used training points to identify the spatial correlations between the dependent (climatological, topography, and local) and independent elements (Slope, LULC and etc.) factors. The frequency ratio model has been used in many places at risk for flooding and insecurity to determine their vulnerability [76–78].

In this study, the following Equation (5) was used to compute the frequency ratio (FR) for each class of all specified parameters to obtain the frequency ratio (FR) for each class:

$$FR = \frac{(\text{PpixE}/\text{PpixT})}{(\Sigma\text{pixE}/\Sigma\text{pixT})} \tag{5}$$

When a flood class is concerned, the number of pixels p in the concerned areas is shown by PpixE, while PpixT represents the total number of pixels in the research area. When a flood class is concerned, the number of pixels is shown by ΣpixE, and the total number of pixels is shown by ΣpixT. When a flood class is concerned, the number of pixels is shown by pixE. It was determined that an appropriate and robust link existed between the flood training points and the relevant factor and high flood risk class implicated if the resultant value of FR was more than 1.0. A value of FR less than 1 indicated a negative relationship and a low flood risk relevance [40]. In the present study, the FR value for each class was considered the specified class weight value (SCWV). The flood vulnerability index (FVI) was also developed to demonstrate the increased relevance of flood susceptibility in the present AHP and FR model analyses, ranging from extremely high to shallow flood risk locations. To compute the FVI using the following Equation (6), the SCWV representing each class of all the specified variables, as well as the SFWV selected for flood events, were taken into consideration:

$$FSI = \sum_{n=1}^{n} (w_i \times FR) \tag{6}$$

SFWV is the weight of variables (i.e., the total number of variables), and *FR* is the frequency ratio value of each class in this equation (i.e., the total number of variables = 7). (i.e., the SCWV).

4.5. Validation

The Area Under the Curve (AUC) method was used to validate the flood susceptibility map of the Mfoundi watershed. This simple method, based on the verification of past occurrences and scientifically justified, allows the accuracy of the AHP model to be verified. It has already been used in several studies and is considered the most appropriate method to validate AHP models [79,80]. For the present study, the AHP-based flood susceptibility map (FHI) was subdivided into 100 classes and the number of pixels belonging to each class was determined. The flood occurrence points were then overlaid on the resulting map, and the number of flood occurrences for each class was listed. Based on this, the cumulative area of the different classes (plotted on the "X" axis) and the cumulative number of flood occurrences (plotted on the "Y" axis) were calculated on a normalized scale from 0 to 1. Then, we calculated the Area Under the Curve (AUC) using the Equation (7) [80]:

$$AUC = \sum_{i=1}^{n=100} \frac{(X_1 + X_2)}{2(Y_2 + Y_1)} \tag{7}$$

where: X denotes the cumulative percentage of the area (highest to lowest); Y denotes the cumulative percentage of flood occurrences; 1 and 2 are two sequential classes of data and n is the number of classes (for our study, n = 100). The AUC value ranges from 0.00 to 1.00, where 0.50–0.60 indicates low accuracy; 0.61–0.70 indicates moderate accuracy; 0.71–0.80 indicates good accuracy; 0.81–0.90 indicates very good accuracy; and 0.91–1.00 indicates excellent accuracy [81].

5. Results

5.1. Effect Weight of Each Class of Flash Flood Susceptibility Variables Found Using the FR Method

Flood susceptibility mapping is an approach for making plans and managing pre-hazards needed to decrease the risk factors. Because of the high altitude, the region of Chaj Doab is often called a flood-prone location. There are many signs of catastrophic flooding with some intervals and return dates. This study highlighted the analysis of flood vulnerability based on a decision-making approach, i.e., an analytic hierarchy process and frequency ratio. Several independent causes induce or condition flooding and play essential roles in flood evaluation. Thus, a statistical databank was prepared for all eight selected conditioning factors (river distance, drainage density, slope, elevation, rainfall, soil, geology, and LULC) with the corresponding subclasses (Figure 3e). Their spatial relations with flood risk were calculated precisely and are given below. Relationships between flood-susceptible and flood-inducing variables were made to allow spatial comparisons between flood-susceptible regions and flood-inducing variables. In this respect, the class weight and factor weight values were considered [82]. A factor's weight value shows the relative significance of each factor chosen and determined using the AHP. The class's weight value shows the importance based on each factor for every individual class and provides valuable details for understanding the role of flood generation.

Based on the quantitative analysis of the relationships between these sites of historic flooding, topographical and geo-environmental variables influencing flash flood events, each variable type's impact weight was determined (Figure 5). The study showed that the altitude class vector's maximum weight belonged to the 500–3500 m elevation class. The weight for a slope above 45° was the maximum weight for the angle of the soil slope. The northwest slope orientation has a greater weight than the other slope directions. Weights significantly influenced the vector distance from the fault class of 400 to 500 m than in other groups. An examination of the river's vector distance found that much of the weight associated with the flood was in the 2500 m class [83]. As seen in Table 3, the rainfall layer had the second-highest weight. This implies that the threshold value for the frequency of flash flooding belonged to this rainfall class. Higher rainfall than this value may also cause flash flooding in conjunction with other variables depending on the length. The vegetation and residential land-use types and being situated next to the river area and on moderate slopes had the highest weighting factors relative to other land uses [84]. Geological research shows that the soil's weight at the beginning is greater than that of the rocky outcrops. The geology had a more significant weight than other parameters in this area.
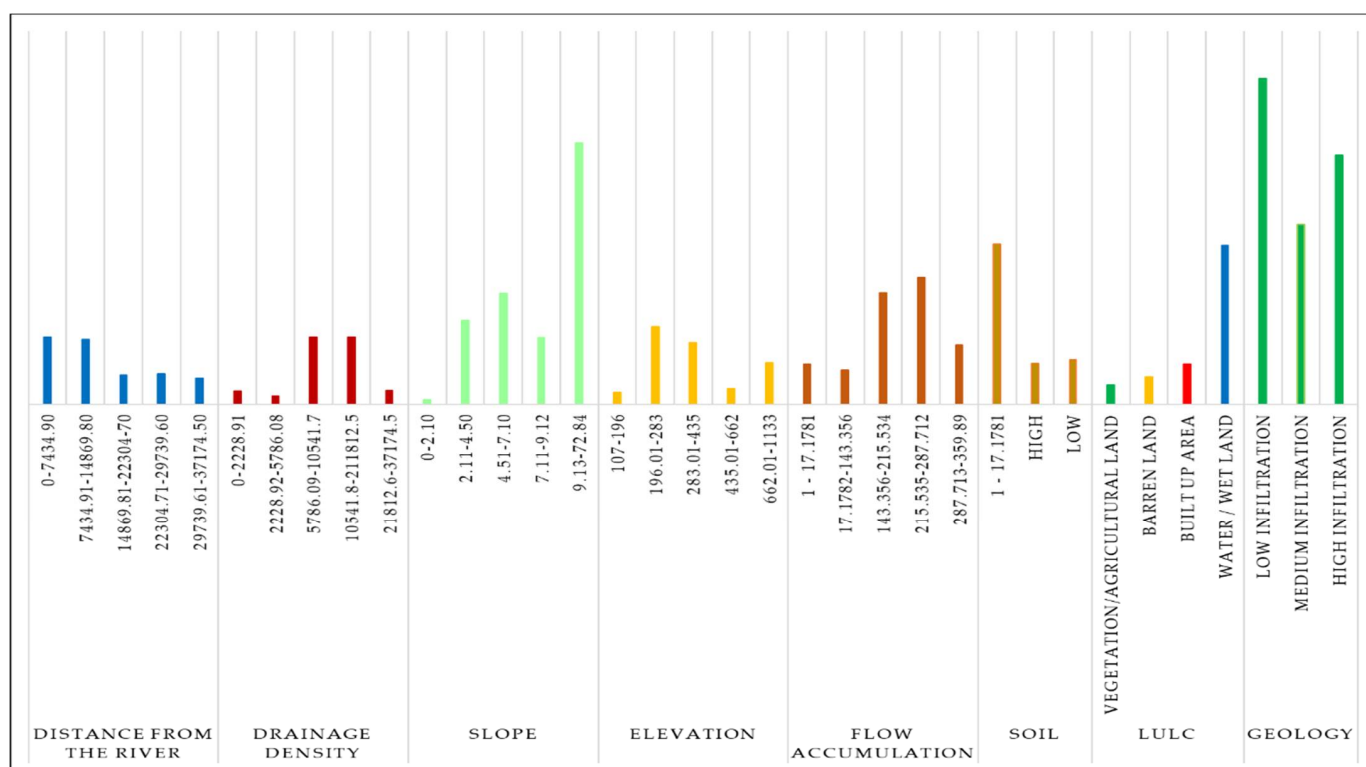
Figure 5. Flood-inducing factors for mapping flood susceptibility based on class frequency ratios.

Table 3. The flood-causing factors and their chosen factor weight values (SFWVs) are presented in the flood susceptibility mapping only for clarification.

S. No	Classes (Abbreviations)	SL	E	DD	R	LULC	DS	G	S	SFWV
1	Slope (SL)	1	0.2	5	4	2	1	4	0.30	0.0152
2	Elevation (E)	1	0.23	0.9	5	1	4	2	0.30	0.0254
3	Drainage Density (DD)	2	5	4	0.2	1	5	3	1	0.2569
4	Rainfall (R)	0.25	0.12	1	0.23	0.5	1	1	0.30	0.0452
5	Landuse/cover (LULC)	0.1	0.12	0.17	0.45	0.5	0.13	0.25	1	0.14
6	Distance from stream (DS)	1	1	3	5	3	5	4	1	0.2592
7	Geology (G)	0.34	0.23	0.25	1	0.25	0.18	2	0.35	0.1190
8	Soil (So)	0.25	4	0.25	1	2	4	3	1	0.18

5.2. Relationships between Flood Susceptibility and Flood-Inducing Factors

Efforts were made to associate flood-susceptible zones and flood-inducing factors spatially. Factor weight values were measured. Rainfall, drought, and floods are closely related (a positive range indicates more than normal rainfall, and a negative range indicates less than normal rainfall). The factor's weight value shows the relative significance of each factor chosen and determined using the AHP. The class's weight value indicates the relative importance of individual classes for each factor and provides valuable details to understand the role of flood generation. The individual class frequency ratio for each factor is shown in Figure 5.

In terms of climate, rainfall still plays an essential part in the study of flood vulnerability. To identify the risk of flooding, rainfall variance was taken into consideration because rainfall deviation is considered the best predictor of flood areas. Figure 3d,e show a variation in rainfall ranging from 918 to 1139 mm, with an FR value of 1, indicating these regions were more prone to floods than low-rainfall-deviated areas [85]. The FR values for

land elevation between 2 and 5 m were >1, suggesting a favorable association with flood vulnerability. The angle of the slope of the sample area ranged from 8° to 45°.

The estimated FR value was between 2.077 and 4.91 in the slope gradient between 45° and 16–30°, suggesting that this section was strongly prone to flooding. In the places along the riverbank, the flood rate was more significant and less so in those regions far away from the river. The analysis of proximity was conducted to produce a specific river distance interval. This analysis shows that a distance of 2500 m from the river has values of FR ranging from 0.54, 0.56, 1.21, 1.26, and 0.48, respectively, which shows that the areas far from the river had lower FR values, meaning a lower risk of flooding.

5.3. Susceptibility Mapping of Flood and Estimation of Risk Area

First, final susceptibility zones were generated in GIS environments via an overlay analysis based on the values of the factor weights and the class values collected from the FR and AHP analyses. The SCWV of each subset of all chosen factors was used for the same variables, as seen in Figure 6. The flood susceptibility index (FSI) was then determined by summing up the FR value for every flood-causing factor identified. A higher FSI value indicates a greater susceptibility to flooding events. Conversely, lower FSI values suggest less exposure to the occurrence of flooding. To recognize the Chaj Doab spatial flood risk zones, the FSI database was reclassified into five susceptibility zones. The output zones were categorized into very low, low, moderate, high, and very high risk, covering 7354, 5147, 3665, 2592, and 1343 km^2, respectively (Figure 5 and Table 4). Some severely damaged villages were identified during the affected areas' visits (Figure 6).
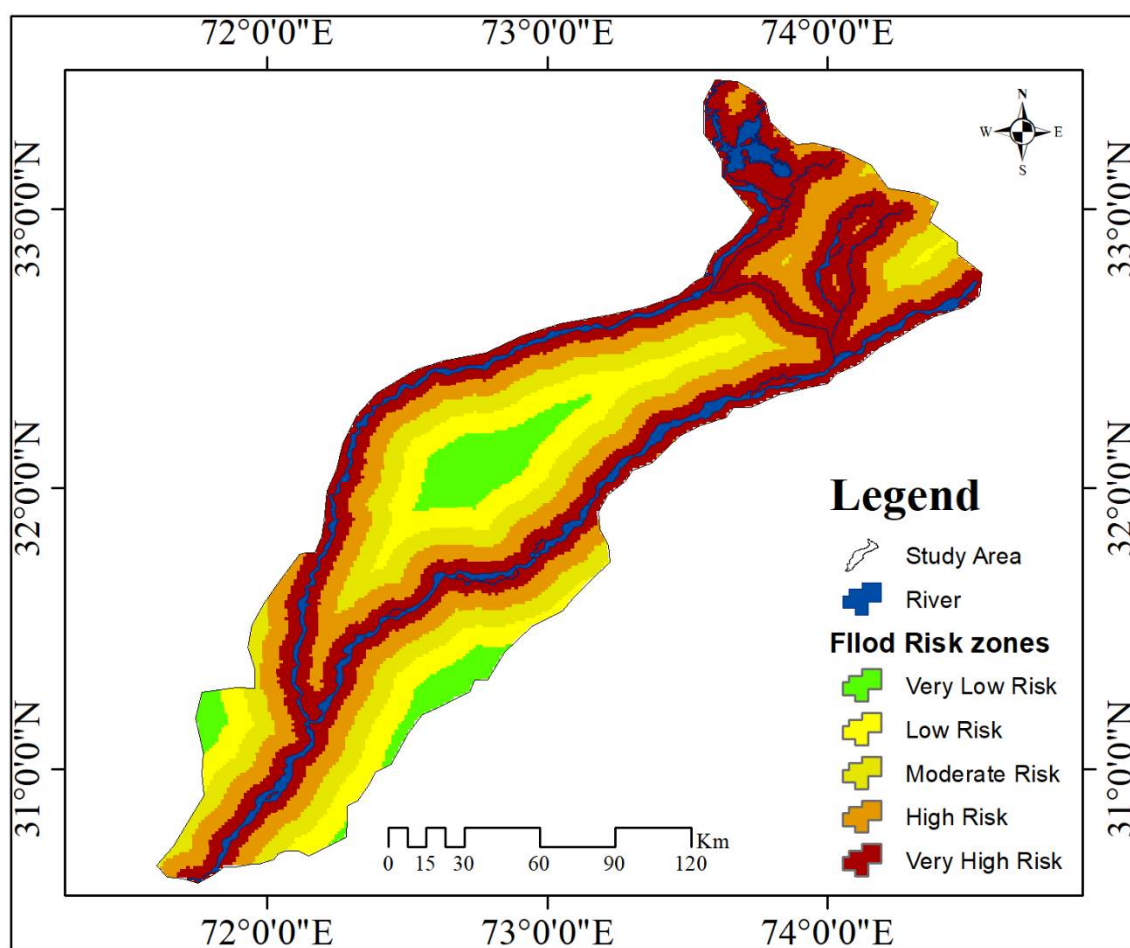

Figure 6. Flood risk zones map of the study area using the AHP and FR models.

Table 4. Flood susceptibility risk classes and estimated area in square kilometers and percentages.

Value	Class	Estimated Risk Area (km²)	Estimated Risk Area (%)
1	Very low risk	7354	36.59
2	Low risk	5147	25.61
3	Moderate risk	3665	18.23
4	High risk	2592	12.89
5	Very high risk	1343	6.68
	Total area	20,101.00	100

Riverside areas of Jhelum, Chinot, Gujrat, and Mandi Bahuddin were at high flood risk. Second, parts of the western side of Jhelum, Chinot, Gujrat, and Mandi Bahuddin were identified as having low to shallow susceptibility to flooding. The low to high susceptibility classes for flooding suggests that these regions are more susceptible to incidences of severe floods.

5.4. Validation Analysis of Risky Zone of the Study Area

From the past literature, it has been concluded that Chaj Doab was entirely washed by the flash flood of 2015. And according to weightage overly and AHP, the final map shows the area susceptible, which is the same area that was hit by the 2015 Jhelum and Chenab flash floods. From ALOSPALSAR DEM, the drainage density was examined as the most critical factor responsible for flash floods in the study area. Drainage density is expressed as the total length of the stream network per unit area [86]. Wazirabad, Chinote, Gujrat, and Mandi Bahuddin are the three main rivers in the study area that are more dangerous because of how much water they have.

When the density increases, the water absorption capacity decreases. Furthermore, five small rivers add water from the right side of the river bank to the main river, increasing the main river's flow level and causing flash floods. In addition, the soil is also one of the critical factors responsible for floods occurring in the study area. While steep slopes increase the chances of flooding, sandy soil absorbs water quickly, and little runoff occurs. On the other hand, clay soils are less porous and hold water longer than sandy soils. This implies that areas characterized by clay soils are more affected by flooding [55]. Geology is not underestimated, and this study, which is an essential factor for flooding in the study area, looked at different rock formations. In contrast, mainly, the area has granite and sediment rocks, which are more resistant to water percolation. High flood zone areas are primarily used for farming, scoring low on a risk scale.

The geology weighting procedure might be inappropriate during the correlation of the pairwise matrix to decide the relative significance of the used elements. This weighting procedure may necessitate a specialist contacting a geology master. The last explanation is that the goals of the information utilized in the current investigation might not sufficiently represent the physical qualities of flood-inclined territories.

The validation of the flood susceptibility map generated by the AHP and FR approach coupled with GIS was based on the AUC of past flood occurrence points in the study area (Figure 6). The high AUC value of AHP and FR (90% and 85%) obtained demonstrates a very good accuracy of the flood susceptibility map of the Chaj Doab (Figure 7). This AUC value is similar to those obtained by Waqas et al. (2021) and Khosravi et al. (2016) respectively for the flood susceptibility mapping of Chitral, Pakistan and Iran (applied to 8 factors). The AUC value obtained in the present study is within the wide range of values obtained in the other study cases. However, the accuracy of the final map obtained in this study accurately verifies the methodology adopted. Therefore, the latter provides a baseline information, which should be taken into account in the urbanization plan, but also in the flood management measures by the decision makers.
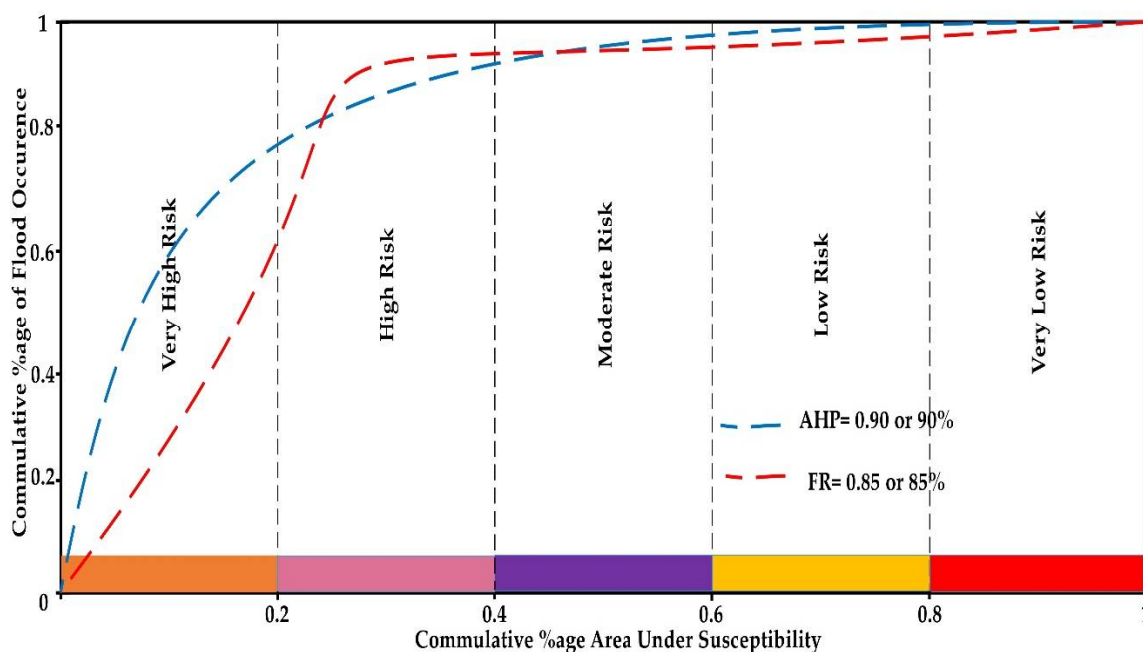
Figure 7. Area Under the Curve (AUC) related to susceptibility model validation of AHP and FR.

6. Discussion

This research presents an experimental methodology for mapping susceptibility to flooding in study areas by joining AHP, FR, and GIS systems techniques with the utilization of MCA [85]. It has been concluded that this research work has demonstrated an experimental approach toward the susceptibility of mapping floods in the study area based on the integration of GIS and AHP techniques for which spatial modeling has been carried out in the environment of GIS [83,84]. The principal motivation behind the present research study is to demonstrate flood risk zones in the north-eastern part of Pakistan. Eight parameters have been chosen to decide the weight of the relative significance utilizing pairwise matrix correlation [12]. For the study area, a flood risk map has been determined using a multi-parametric methodology that results in the susceptible zones by utilizing morphometric and topographic factors. A 0.04 consistency ratio was determined from this process. It has been stated that CR > 0.1 indicates that the judgment is at the limit of consistency, though CRs > 0.1 (but not too much more) have to be accepted sometimes. In this instance, we are on safe ground. A CR as high as, say, 0.9 would mean that the pairwise judgments are just about random and are entirely untrustworthy. The results show that the areas covered are 1343 km^2, of which 6.68% are very high risk to the total area [12]. Differences in characteristics—such as the location of the study area, the characteristics of regional rainfall, selection of climate model data, model downscaling methods, subsurface, and hydrological elements—can lead to different predicted risk results [42–47].

According to expert opinion and the author score from AHP, Mandi Bahudin, Jhang, and Sargodha are more vulnerable to flash floods. In the areas mentioned above, there is a high risk of flooding. The outcomes of creating flood zones using the analytical hierarchy process will be explored in future research that incorporates other physical elements. As a result, the weighting of relative significance factors must be quickly changed because of changes in the variables relevant to the study [87,88]. The flood hazard map was developed, and each parameter was assigned a value. Summation and division were used to remove all of the specified values. A set of final values and appropriate weights were determined. The data on land use values, slope, density, geology, soil, and observed geographical circumstances were utilized to assess the degree of susceptibility in the research region [89,90]. As with creating a flood danger map, precise numerical values were assigned to these indications. In addition, the weightage values for each of these

numbers were also included. There were four different categories: "very high", "medium", "low", and "flood-free". ArcGIS tools were used to make a map of the flood danger zones. Differences in disaster exposure values, the change of region vulnerability, and correction methods of data will lead to differences in the results of risk assessment [25,26,40,41].

Despite some imperfections related to the quality of the medium resolution image (Sentinel-2) used in the present study, the subjectivity of the coastlines attributed/assigned to certain parameters, the fact remains that the flood susceptibility map of the Chaj Doab obtained constitutes a real tool for development, planning and decision-making by the administrative authorities and the decentralized territorial communities with jurisdiction. The results of this work will undoubtedly contribute to the improvement of the living conditions of the populations of this intensely populated area where the problem of environmental management and sanitation constitute a real bottleneck. Indeed, the map obtained in accordance with the field observations. However, it would be necessary in future work to integrate these impertinences and at best, to try out more efficient models capable of reducing the margins of error to a minimum. This work is the first of its kind to use a wide range of environmental data (ALOSPALSAR Dem, rainfall, geology) to assess the susceptibility of the Chaj Doab region to flooding in a context of global change. These results constitute a first step in the search for a solution to the flooding problems in the Chaj Doab; they will also allow the administrative authorities, the government and the decentralized territorial communities and all other development actors to achieve synergy of action in the interventions before, during and after the floods in this region. From a scientific point of view, this work will not only allow us to better understand the environment of the Chaj Doab, but also to identify and evaluate the parameters that control the risk of flooding.

The consequences of this research affirm that the utilization of multi-criteria assessment for various variables is likewise shown to be helpful in the definition of the risk regions for flood mapping and predictions. Generally speaking, the contextual analysis shows that the GIS-MCA-AHP-based class model is robust in flood risk assessment and zonation. The research results declared that integrating GIS and AHP techniques has provided an effective tool for decision-making for flood hazard mapping because it permits the intelligible and influential usage of particular data. For additional research and to take further advantage of AHP in flash flood studies, research efforts could be focused on how AHP can be integrated with other essential techniques like fuzzy logic, etc.

7. Conclusions

This research has demonstrated an experimental approach toward the susceptibility of mapping floods based on the integration of FR and AHP techniques in the northern parts of Punjab, Pakistan. Eight parameters have been chosen to decide the weight of the relative significance, utilizing pairwise matrix correlation. As a result, the weighting of relative significance factors must be quickly changed because of changes in the variables relevant to the study. The flood hazard map was created using ArcGIS algorithms to determine the final product's extremely high, moderate, and low flood zones. Several characteristics were utilized to determine the research region's susceptibility, including data on land use values, slope, density, geology, and soil. Like when creating a flood risk map, these indicators have specific numerical values assigned to them. They were then combined with weightage values, and vulnerable flood zones were created. As a result, flash flood maps were developed by defining the very high to no susceptible zones. The results indicated that the very high flood areas cover 1343 km^2, or 6.68% of the total area. The Mangla, Marala, and Trimmu valleys were identified as high-risk zones of the study area, which have been damaged drastically many times by flash floods. As study limitations we can mention the uncertainties in dataset. Also, we considered only some factors, not all, that affect the extreme rainfall to assess the hazard changes in the study area. The resultant risk mapping provides guidelines for decision-makers to replicate the same for the rest of the country and save the lives and properties of the vulnerable population. Our findings

suggest balancing economic growth, risk management, and risk avoidance is an important issue that needs to be addressed in the long-term development of the area. This proposed approach can also help policymakers and decision-makers evaluate and assess flooding phenomena in study areas. In future studies, the factors that affect extreme rainfall such as regional circulation should also be considered, in order to improve the accuracy of regional extreme rainfall prediction. Moreover, the ensemble method can be used to assess the effect on flash floods.

References

1. Hussain, E.; Ural, S.; Malik, A.; Shan, J. Mapping pakistan 2010 floods using remote sensing data. In Proceedings of the American Society for Photogrammetry and Remote Sensing Annual Conference, Milwaukee, WI, USA, 1–5 May 2011; Volume 2011, pp. 215–222.

2. Yue, Z.; Zhou, W.; Li, T. Impact of the Indian Ocean Dipole on Evolution of the Subsequent ENSO: Relative Roles of Dynamic and Thermodynamic Processes. *J. Clim.* **2021**, *34*, 3591–3607. [CrossRef]

3. Quan, Q.; Gao, S.; Shang, Y.; Wang, B. Assessment of the sustainability of *Gymnocypris eckloni* habitat under river damming in the source region of the Yellow River. *Sci. Total Environ.* **2021**, *778*, 146312. [CrossRef] [PubMed]

4. Zhang, K.; Wang, S.; Bao, H.; Zhao, X. Characteristics and influencing factors of rainfall-induced landslide and debris flow hazards in Shaanxi Province, China. *Nat. Hazards Earth Syst. Sci.* **2019**, *19*, 93–105. [CrossRef]

5. Wang, S.; Zhang, K.; Chao, L.; Li, D.; Tian, X.; Bao, H.; Chen, G.; Xia, Y. Exploring the utility of radar and satellite-sensed precipitation and their dynamic bias correction for integrated prediction of flood and landslide hazards. *J. Hydrol.* **2021**, *603*, 126964. [CrossRef]

6. Wahla, S.S.; Kazmi, J.; Sharifi, A.; Shirazi, S.; Tariq, A.; Smith, H.J. Assessing Spatio-temporal mapping and monitoring of climatic Variability using SPEI and RF machine learning models. *Geocarto Int.* **2022**, 1–22. [CrossRef]

7. Dai, J.; Feng, H.; Shi, K.; Ma, X.; Yan, Y.; Ye, L.; Xia, Y. Electrochemical degradation of antibiotic enoxacin using a novel PbO2 electrode with a graphene nanoplatelets inter-layer: Characteristics, efficiency and mechanism. *Chemosphere* **2022**, *307*, 135833. [CrossRef] [PubMed]

8. Liu, E.; Chen, S.; Yan, D.; Deng, Y.; Wang, H.; Jing, Z.; Pan, S. Detrital zircon geochronology and heavy mineral composition constraints on provenance evolution in the western Pearl River Mouth basin, northern south China sea: A source to sink approach. *Mar. Pet. Geol.* **2022**, *145*, 105884. [CrossRef]

9. Chen, X.; Quan, Q.; Zhang, K.; Wei, J. Spatiotemporal characteristics and attribution of dry/wet conditions in the Weihe River Basin within a typical monsoon transition zone of East Asia over the recent 547 years. *Environ. Model. Softw.* **2021**, *143*, 105116. [CrossRef]

10. Huang, Y.; Bárdossy, A.; Zhang, K. Sensitivity of hydrological models to temporal and spatial resolutions of rainfall data. *Hydrol. Earth Syst. Sci.* **2019**, *23*, 2647–2663. [CrossRef]

11. Tariq, A.; Riaz, I.; Ahmad, Z.; Yang, B.; Amin, M.; Kausar, R.; Andleeb, S.; Farooqi, M.A.; Rafiq, M. Land surface temperature relation with normalized satellite indices for the estimation of spatio-temporal trends in temperature among various land use land cover classes of an arid Potohar region using Landsat data. *Environ. Earth Sci.* **2019**, *79*, 40. [CrossRef]

12. Waqas, H.; Lu, L.; Tariq, A.; Li, Q.; Baqa, M.; Xing, J.; Sajjad, A. Flash Flood Susceptibility Assessment and Zonation Using an Integrating Analytic Hierarchy Process and Frequency Ratio Model for the Chitral District, Khyber Pakhtunkhwa, Pakistan. *Water* **2021**, *13*, 1650. [CrossRef]

13. Tariq, A.; Mumtaz, F.; Zeng, X.; Baloch, M.Y.J.; Moazzam, M.F.U. Spatio-temporal variation of seasonal heat islands mapping of Pakistan during 2000–2019, using day-time and night-time land surface temperatures MODIS and meteorological stations data. *Remote Sens. Appl. Soc. Environ.* **2022**, *27*, 100779. [CrossRef]

14. Zhu, Z.; Wu, Y.; Liang, Z. Mining-Induced Stress and Ground Pressure Behavior Characteristics in Mining a Thick Coal Seam With Hard Roofs. *Front. Earth Sci.* **2022**, *10*, 843191. [CrossRef]

15. Guo, Y.; Yang, Y.; Kong, Z.; He, J. Development of Similar Materials for Liquid-Solid Coupling and Its Application in Water Outburst and Mud Outburst Model Test of Deep Tunnel. *Geofluids* **2022**, *2022*, 8784398. [CrossRef]

16. Liu, Y.; Zhang, Z.; Liu, X.; Wang, L.; Xia, X. Efficient image segmentation based on deep learning for mineral image classification. *Adv. Powder Technol.* **2021**, *32*, 3885–3903. [CrossRef]

17. Chen, Z.; Liu, Z.; Yin, L.; Zheng, W. Statistical analysis of regional air temperature characteristics before and after dam construction. *Urban Clim.* **2022**, *41*, 101085. [CrossRef]

18. Yin, L.; Wang, L.; Keim, B.D.; Konsoer, K.; Zheng, W. Wavelet Analysis of Dam Injection and Discharge in Three Gorges Dam and Reservoir with Precipitation and River Discharge. *Water* **2022**, *14*, 567. [CrossRef]

19. Yin, L.; Wang, L.; Zheng, W.; Ge, L.; Tian, J.; Liu, Y.; Yang, B.; Liu, S. Evaluation of Empirical Atmospheric Models Using Swarm-C Satellite Data. *Atmosphere* **2022**, *13*, 294. [CrossRef]

20. Zhang, X.; Ma, F.; Yin, S.; Wallace, C.D.; Soltanian, M.R.; Dai, Z.; Ritzi, R.W.; Ma, Z.; Zhan, C.; Lü, X. Application of upscaling methods for fluid flow and mass transport in multi-scale heterogeneous media: A critical review. *Appl. Energy* **2021**, *303*, 117603. [CrossRef]

21. Zhan, C.; Dai, Z.; Samper, J.; Yin, S.; Ershadnia, R.; Zhang, X.; Wang, Y.; Yang, Z.; Luan, X.; Soltanian, M.R. An integrated inversion framework for heterogeneous aquifer structure identification with single-sample generative adversarial network. *J. Hydrol.* **2022**, *610*. [CrossRef]

22. Avand, M.; Moradi, H.; Lasboyee, M.R. Spatial modeling of flood probability using geo-environmental variables and machine learning models, case study: Tajan watershed, Iran. *Adv. Space Res.* **2021**, *67*, 3169–3186. [CrossRef]

23. Thomas, V. *Climate Change and Natural Disasters*; Taylor & Francis Group: New York, NY, USA, 2017; Volume 8, pp. 81–94. [CrossRef]

24. Tehrany, M.S.; Lee, M.J.; Pradhan, B.; Jebur, M.N.; Lee, S. Flood susceptibility mapping using integrated bivariate and multivariate statistical models. *Environ. Earth Sci.* **2014**, *72*, 4001–4015. [CrossRef]

25. Costache, R.; Pham, Q.B.; Arabameri, A.; Diaconu, D.C.; Costache, I.; Crăciun, A.; Ciobotaru, N.; Pandey, M.; Arora, A.; Ali, S.A.; et al. Flash-flood propagation susceptibility estimation using weights of evidence and their novel ensembles with multicriteria decision making and machine learning. *Geocarto Int.* **2021**, 1–33. [CrossRef]

26. Khatoon, R.; Hussain, I.; Anwar, M.; Nawaz, M.A. Diet selection of snow leopard (*Panthera uncia*) in Chitral, Pakistan. *Turk. J. Zool.* **2017**, *41*, 914–923. [CrossRef]

27. Huang, S.; Liu, C. A computational framework for fluid–structure interaction with applications on stability evaluation of breakwater under combined tsunami–earthquake activity. *Comput. Civ. Infrastruct. Eng.* **2022**. [CrossRef]

28. Zhou, G.; Long, S.; Xu, J.; Zhou, X.; Song, B.; Deng, R.; Wang, C. Comparison Analysis of Five Waveform Decomposition Algorithms for the Airborne LiDAR Echo Signal. *IEEE J. Sel. Top. Appl. Earth Obs. Remote Sens.* **2021**, *14*, 7869–7880. [CrossRef]

29. Zhou, G.; Zhang, R.; Huang, S. Generalized Buffering Algorithm. *IEEE Access* **2021**, *9*, 27140–27157. [CrossRef]

30. Wang, Q.; Zhou, G.; Song, R.; Xie, Y.; Luo, M.; Yue, T. Continuous space ant colony algorithm for automatic selection of orthophoto mosaic seamline network. *ISPRS J. Photogramm. Remote Sens.* **2022**, *186*, 201–217. [CrossRef]

31. Wang, P.; Wang, L.; Leung, H.; Zhang, G. Super-Resolution Mapping Based on Spatial–Spectral Correlation for Spectral Imagery. *IEEE Trans. Geosci. Remote Sens.* **2020**, *59*, 2256–2268. [CrossRef]

32. Tian, H.; Qin, Y.; Niu, Z.; Wang, L.; Ge, S. Summer Maize Mapping by Compositing Time Series Sentinel-1A Imagery Based on Crop Growth Cycles. *J. Indian Soc. Remote Sens.* **2021**, *49*, 2863–2874. [CrossRef]

33. Tian, H.; Wang, Y.; Chen, T.; Zhang, L.; Qin, Y. Early-Season Mapping of Winter Crops Using Sentinel-2 Optical Imagery. *Remote Sens.* **2021**, *13*, 3822. [CrossRef]

34. Tian, H.F.; Huang, N.; Niu, Z.; Qin, Y.C.; Pei, J.; Wang, J. Mapping Winter Crops in China with Multi-Source Satellite Imagery and Phenology-Based Algorithm. *Remote Sens.* **2019**, *11*, 820. [CrossRef]

35. Avand, M.; Moradi, H.R.; Ramazanzadeh Lasboyee, M. Spatial Prediction of Future Flood Risk: An Approach to the Effects of Climate Change. *Geoscience* **2021**, *11*, 25. [CrossRef]

36. Tian, H.; Pei, J.; Huang, J.; Li, X.; Wang, J.; Zhou, B.; Qin, Y.; Wang, L. Garlic and Winter Wheat Identification Based on Active and Passive Satellite Imagery and the Google Earth Engine in Northern China. *Remote Sens.* **2020**, *12*, 3539. [CrossRef]

37. Luan, D.; Liu, A.; Wang, X.; Xie, Y.; Wu, Z. Robust Two-Stage Location Allocation for Emergency Temporary Blood Supply in Postdisaster. *Discret. Dyn. Nat. Soc.* **2022**, *2022*, 6184170. [CrossRef]

38. Chen, J.; Du, L.; Guo, Y. Label constrained convolutional factor analysis for classification with limited training samples. *Inf. Sci.* **2020**, *544*, 372–394. [CrossRef]

39. Tariq, A.; Shu, H. CA-Markov Chain Analysis of Seasonal Land Surface Temperature and Land Use Landcover Change Using Optical Multi-Temporal Satellite Data of Faisalabad, Pakistan. *Remote Sens.* **2020**, *12*, 3402. [CrossRef]

40. Bui, D.T.; Tsangaratos, P.; Ngo, P.-T.T.; Pham, T.D.; Pham, B.T. Flash flood susceptibility modeling using an optimized fuzzy rule based feature selection technique and tree based ensemble methods. *Sci. Total Environ.* **2019**, *668*, 1038–1054. [CrossRef]

41. Hoang, L.P.; Biesbroek, R.; Tri, V.P.D.; Kummu, M.; van Vliet, M.T.H.; Leemans, R.; Kabat, P.; Ludwig, F. Managing flood risks in the Mekong Delta: How to address emerging challenges under climate change and socioeconomic developments. *Ambio* **2018**, *47*, 635–649. [CrossRef]

42. Liu, M.; Chen, N.; Zhang, Y.; Deng, M. Glacial Lake Inventory and Lake Outburst Flood/Debris Flow Hazard Assessment after the Gorkha Earthquake in the Bhote Koshi Basin. *Water* **2020**, *12*, 464. [CrossRef]

43. Kirkby, M.; Bracken, L.; Reaney, S. The influence of land use, soils and topography on the delivery of hillslope runoff to channels in SE Spain. *Earth Surf. Process. Landf.* **2002**, *27*, 1459–1473. [CrossRef]

44. European Environmental Agency. *Mapping the Impacts of Natural Hazards and Technological Accidents in Europe: An Overview of the Last Decade*; Publications Office of the European Union: Luxembourg, 2010; ISBN 978-92-9213-168-5.

45. Aoki, K.; Uehara, M.; Kato, C.; Hirahara, H. Evaluation of Rugby Players' Psychological-Competitive Ability by Utilizing the Analytic Hierarchy Process. *Open J. Soc. Sci.* **2016**, *4*, 103–117. [CrossRef]

46. Alexakis, D.D.; Sarris, A. Integrated GIS and remote sensing analysis for landfill sitting in Western Crete, Greece. *Environ. Earth Sci.* **2013**, *72*, 467–482. [CrossRef]

47. Ahmad, D.; Afzal, M. Flood hazards and factors influencing household flood perception and mitigation strategies in Pakistan. *Environ. Sci. Pollut. Res.* **2020**, *27*, 15375–15387. [CrossRef] [PubMed]

48. Li, Y.; Du, L.; Wei, D. Multiscale CNN Based on Component Analysis for SAR ATR. *IEEE Trans. Geosci. Remote Sens.* **2021**, *60*, 1–12. [CrossRef]

49. Zhao, M.; Zhou, Y.; Li, X.; Cheng, W.; Zhou, C.; Ma, T.; Li, M.; Huang, K. Mapping urban dynamics (1992–2018) in Southeast Asia using consistent nighttime light data from DMSP and VIIRS. *Remote Sens. Environ.* **2020**, *248*, 111980. [CrossRef]

50. Zhao, M.; Zhou, Y.; Li, X.; Zhou, C.; Cheng, W.; Li, M.; Huang, K. Building a Series of Consistent Night-Time Light Data (1992–2018) in Southeast Asia by Integrating DMSP-OLS and NPP-VIIRS. *IEEE Trans. Geosci. Remote Sens.* **2019**, *58*, 1843–1856. [CrossRef]

51. Muhammad Ishaq, I. ullah Political/Power Structure and Vulnerability to Natural Disaster in North Western Pakistan. *Res. J. Soc. Sci. Econ. Rev.* **2020**, *1*, 389–400.

52. Dewan, T.H. Societal impacts and vulnerability to floods in Bangladesh and Nepal. *Weather Clim. Extrem.* **2014**, *7*, 36–42. [CrossRef]

53. Soriano, I.R.; Prot, J.C.; Matias, D.M. Expression of Tolerance for *Meloidogyne graminicola* in Rice Cultivars as Affected by Soil Type and Flooding. *J. Nematol.* **2000**, *32*, 309–317.

54. Costache, R.; Tin, T.T.; Arabameri, A.; Crăciun, A.; Ajin, R.; Costache, I.; Islam, A.R.M.T.; Abba, S.; Sahana, M.; Avand, M.; et al. Flash-flood hazard using deep learning based on H$_2$O R package and fuzzy-multicriteria decision-making analysis. *J. Hydrol.* **2022**, *609*, 127747. [CrossRef]

55. Ouma, Y.O.; Tateishi, R. Urban Flood Vulnerability and Risk Mapping Using Integrated Multi-Parametric AHP and GIS: Methodological Overview and Case Study Assessment. *Water* **2014**, *6*, 1515–1545. [CrossRef]

56. Ali, S.A.; Khatun, R.; Ahmad, A.; Ahmad, S.N. Application of GIS-based analytic hierarchy process and frequency ratio model to flood vulnerable mapping and risk area estimation at Sundarban region, India. *Model. Earth Syst. Environ.* **2019**, *5*, 1083–1102. [CrossRef]

57. Pradhan, B.; Chaudhari, A.; Adinarayana, J.; Buchroithner, M.F. Soil erosion assessment and its correlation with landslide events using remote sensing data and GIS: A case study at Penang Island, Malaysia. *Environ. Monit. Assess.* **2011**, *184*, 715–727. [CrossRef] [PubMed]

58. Strahler, A.N. Dynamic basis of geomorphology. *Bull. Geol. Am.* **1952**, *63*, 923–939. [CrossRef]

59. Ghezelsofloo, A.A.; Hajibigloo, M. Application of Flood Hazard Potential Zoning by using AHP Algorithm. *Civ. Eng. Res. J.* **2020**, *9*, 150–159. [CrossRef]

60. Pimentel, S.; Flowers, G.E. A numerical study of hydrologically driven glacier dynamics and subglacial flooding. *Proc. R. Soc. A Math. Phys. Eng. Sci.* **2010**, *467*, 537–558. [CrossRef]

61. Khan, B.; Iqbal, M.J.; Yosufzai, M.A.K. Flood risk assessment of River Indus of Pakistan. *Arab. J. Geosci.* **2010**, *4*, 115–122. [CrossRef]

62. Ashraf, M.; Bhatti, M.T.; Shakir, A.S. River bank erosion and channel evolution in sand-bed braided reach of River Chenab: Role of floods during different flow regimes. *Arab. J. Geosci.* **2016**, *9*, 140. [CrossRef]

63. Yariyan, P.; Avand, M.; Abbaspour, R.A.; Torabi Haghighi, A.; Costache, R.; Ghorbanzadeh, O.; Janizadeh, S.; Blaschke, T. Flood susceptibility mapping using an improved analytic network process with statistical models. *Geomat. Nat. Hazards Risk* **2020**, *11*, 2282–2314. [CrossRef]

64. Talukdar, S.; Ghose, B.; Shahfahad; Salam, R.; Mahato, S.; Pham, Q.B.; Linh, N.T.T.; Costache, R.; Avand, M. Flood susceptibility modeling in Teesta River basin, Bangladesh using novel ensembles of bagging algorithms. *Stoch. Hydrol. Hydraul.* **2020**, *34*, 2277–2300. [CrossRef]

65. Avand, M.; Kuriqi, A.; Khazaei, M.; Ghorbanzadeh, O. DEM resolution effects on machine learning performance for flood probability mapping. *J. Hydro-Environ. Res.* **2021**, *40*, 1–16. [CrossRef]

66. Elkhrachy, I. Vertical accuracy assessment for SRTM and ASTER Digital Elevation Models: A case study of Najran city, Saudi Arabia. *Ain Shams Eng. J.* **2018**, *9*, 1807–1817. [CrossRef]

67. Giordan, D.; Notti, D.; Zucca, F.; Pepe, A.; Villa, A.; Calò, F.; Pepe, A.; Dutto, F.; Pari, P.; Baldo, M.; et al. Low cost, multiscale and multi-sensor application for flooded area mapping Low Strain rates area monitoring with AInSAR and GPS View project alpsmotion View project Low cost, multiscale and multi-sensor application for flooded area mapping. *Nat. Hazards Earth Syst. Sci.* **2018**, *18*, 1493–1516. [CrossRef]

68. Samanta, S.; Kumar Pal, D.; Palsamanta, B. Flood susceptibility analysis through remote sensing, GIS and frequency ratio model. *Appl. Water Sci.* **2018**, *8*, 66. [CrossRef]

69. Atif, I.; Mahboob, M.A.; Waheed, A. Spatio-Temporal Mapping and Multi-Sector Damage Assessment of 2014 Flood in Pakistan using Remote Sensing and GIS. *Indian J. Sci. Technol.* **2016**, *8*, 1–18. [CrossRef]

70. Sajjad, A.; Lu, J.Z.; Chen, X.L.; Chisenga, C.; Mahmood, S. The riverine flood catastrophe in August 2010 in south Punjab, Pakistan: Potential causes, extent and damage assessment. *Appl. Ecol. Environ. Res.* **2019**, *17*, 14121–14142. [CrossRef]

71. Samboko, H.T.; Abas, I.; Luxemburg, W.M.J.; Savenije, H.H.G.; Makurira, H.; Banda, K.; Winsemius, H.C. Evaluation and improvement of remote sensing-based methods for river flow management. *Phys. Chem. Earth* **2020**, *117*, 102839. [CrossRef]

72. Zhao, G.; Pang, B.; Xu, Z.; Peng, D.; Xu, L. Assessment of urban flood susceptibility using semi-supervised machine learning model. *Sci. Total Environ.* **2019**, *659*, 940–949. [CrossRef]

73. Markantonis, V.; Meyer, V.; Lienhoop, N. Evaluation of the environmental impacts of extreme floods in the Evros River basin using Contingent Valuation Method. *Nat. Hazards* **2013**, *69*, 1535–1549. [CrossRef]

74. Saaty, T.L. A scaling method for priorities in hierarchical structures. *J. Math. Psychol.* **1977**, *15*, 234–281. [CrossRef]

75. Le, L.M.; Ly, H.B.; Pham, B.T.; Le, V.M.; Pham, T.A.; Nguyen, D.H.; Tran, X.T.; Le, T.T. Hybrid artificial intelligence approaches for predicting buckling damage of steel columns under axial compression. *Materials* **2019**, *12*, 1670. [CrossRef] [PubMed]

76. Stedinger, J.R.; Vogel, R.M.; Foufoula-Georgiou, E. Frequency Analysis of Extreme Events. *Handb. Hydrol.* **1993**, *18*, 1.

77. Ullah, K.; Zhang, J. GIS-based flood hazard mapping using relative frequency ratio method: A case study of panjkora river basin, eastern Hindu Kush, Pakistan. *PLoS ONE* **2020**, *15*, e0229153. [CrossRef]

78. Jung, Y.; Merwade, V.; Yeo, K.; Shin, Y.; Lee, S.O. An approach using a 1D hydraulic model, landsat imaging and generalized likelihood uncertainty estimation for an approximation of flood discharge. *Water* **2013**, *5*, 1598–1621. [CrossRef]

79. Rahman, M.; Ningsheng, C.; Mahmud, G.I.; Islam, M.M.; Pourghasemi, H.R.; Ahmad, H.; Habumugisha, J.M.; Washakh, R.M.A.; Alam, M.; Liu, E.; et al. Flooding and its relationship with land cover change, population growth, and road density. *Geosci. Front.* **2021**, *12*, 101224. [CrossRef]

80. Das, S. Geospatial mapping of flood susceptibility and hydro-geomorphic response to the floods in Ulhas basin, India. *Remote Sens. Appl. Soc. Environ.* **2019**, *14*, 60–74. [CrossRef]

81. Yesilnacar, E.; Topal, T. Landslide susceptibility mapping: A comparison of logistic regression and neural networks methods in a medium scale study, Hendek region (Turkey). *Eng. Geol.* **2005**, *79*, 251–266. [CrossRef]

82. Duc, T.T. Using Gis and Ahp Technique for Land-Use Suitability Analysis. Int. Symp. Geoinform. Spat. Infrastruct. *Dev. Earth Allied Sci.* **2006**, 1–6.

83. Bozdağ, A.; Yavuz, F.; Günay, A.S. AHP and GIS based land suitability analysis for Cihanbeyli (Turkey) County. *Environ. Earth Sci.* **2016**, *75*, 813. [CrossRef]

84. Kayastha, P.; Dhital, M.R.; De Smedt, F. Application of the analytical hierarchy process (AHP) for landslide susceptibility mapping: A case study from the Tinau watershed, west Nepal. *Comput. Geosci.* **2013**, *52*, 398–408. [CrossRef]

85. Siddayao, G.P.; Valdez, S.E.; Fernandez, P.L. Analytic Hierarchy Process (AHP) in Spatial Modeling for Floodplain Risk Assessment. *Int. J. Mach. Learn. Comput.* **2014**, *4*, 450–457. [CrossRef]

86. Mondal, S.; Maiti, R. Integrating the Analytical Hierarchy Process (AHP) and the frequency ratio (FR) model in landslide susceptibility mapping of Shiv-khola watershed, Darjeeling Himalaya. *Int. J. Disaster Risk Sci.* **2013**, *4*, 200–212. [CrossRef]

87. Khosravi, K.; Nohani, E.; Maroufinia, E.; Pourghasemi, H.R. A GIS-based flood susceptibility assessment and its mapping in Iran: A comparison between frequency ratio and weights-of-evidence bivariate statistical models with multi-criteria decision-making technique. *Nat. Hazards* **2016**, *83*, 947–987. [CrossRef]

88. Islam, M.M.; Ujiie, K.; Noguchi, R.; Ahamed, T. Flash flood-induced vulnerability and need assessment of wetlands using remote sensing, GIS, and econometric models. *Remote Sens. Appl. Soc. Environ.* **2022**, *25*, 100692. [CrossRef]

89. Roopnarine, R.; Opadeyi, J.; Eudoxie, G.; Thong, G.; Edwards, E. GIS-based flood susceptibility and risk mapping Trinidad using weight factor modeling. *Caribb. J. Earth Sci.* **2018**, *49*, 1–9.

90. Qadir, A.; Malik, R.N.; Husain, S.Z. Spatio-temporal variations in water quality of Nullah Aik-tributary of the river Chenab, Pakistan. *Environ. Monit. Assess.* **2008**, *140*, 43–59. [CrossRef]